Title

Quantitative parameters of intravoxel incoherent motion diffusion weighted imaging (IVIM-DWI): potential application in predicting pathological grades of pancreatic ductal adenocarcinoma.

Journal

Quantitative imaging in medicine and surgery, 8(3)

ISSN

2223-4292

Authors

Ma, Wanling
Zhang, Guangwen
Ren, Jing
et al.

Publication Date

2018-04-01

DOI

10.21037/qims.2018.04.08

Peer reviewed

Original Article

Quantitative parameters of intravoxel incoherent motion diffusion weighted imaging (IVIM-DWI): potential application in predicting pathological grades of pancreatic ductal adenocarcinoma

Wanling Ma[1#], Guangwen Zhang[1#], Jing Ren[1], Qi Pan[1], Didi Wen[1], Jinman Zhong[1], Zhuoli Zhang[2], Yi Huan[1]

[1]Department of Radiology, Xijing Hospital, Fourth Military Medical University, Xi'an 710032, China; [2]Department of Radiology, Feinberg School of Medicine, Northwestern University, Chicago, IL 60611, USA

[#]These authors contributed equally to this work.

Correspondence to: Yi Huan, MD, PhD. Department of Radiology, Xijing Hospital, Fourth Military Medical University, Changle West Road 127#, Xi'an 710032, China. Email: huanyi3000@163.com.

Background: The aim of this study was to compare intravoxel incoherent motion diffusion weighted imaging (IVIM-DWI) parameters such as standard apparent diffusion coefficient ($ADC_{standard}$), pure diffusion coefficient (D_{slow}), pseudodiffusion coefficient (D_{fast}) and perfusion fraction (f) for differentiating pancreatic ductal adenocarcinoma (PDAC) with different pathological grades.

Methods: Institutional Review Board of our hospital approved this study protocol. Subjects comprised 38 PDACs confirmed by pathology. Pancreatic multiple b values DWI with 15 b values of 0, 10, 20, 40, 60, 80, 100, 150, 200, 400, 800, 1,000, 1200, 1,500, and 2,000 s/mm^2 was performed using GE Discovery MR750 3.0T scanner. $ADC_{standard}$, D_{slow}, D_{fast} and f values of all PDACs were calculated using mono- and bi-exponential models. Parameters of well/moderately differentiated and poorly differentiated PDAC were compared using Independent Sample t-test. P values <0.05 were considered significant.

Results: Mean D_{slow} value of well/moderately differentiated PDAC was significantly lower than that of poorly differentiated PDAC (0.540×10^{-3} *vs.* 0.676×10^{-3} mm^2/s, P<0.001). Mean f value of well/moderately differentiated PDAC was significantly higher than that of poorly differentiated PDAC (60.3% *vs.* 38.4%, P<0.001). The area under curve value of f in differentiating well/moderately differentiated PDAC from poorly differentiated PDAC was slightly higher than that of D_{slow} (0.894>0.865). When the D_{slow} value was less than or equal to 0.599×10^{-3} mm^2/s, the sensitivity and specificity were 100% and 84.6% respectively. When f value was greater than 49.6%, the sensitivity and specificity were 92.0% and 84.6% respectively.

Conclusions: D_{slow} and f derived from IVIM-DWI model can be used to distinguish well/moderately differentiated PDAC from poorly differentiated PDAC. And to serve this purpose, D_{slow} and f have high diagnostic performance. IVIM-DWI is a promising and non-invasive tool for predicting pathological grade of PDAC.

Keywords: Pancreatic ductal adenocarcinoma (PDAC); intravoxel incoherent motion; pure diffusion coefficient; pseudodiffusion coefficient; perfusion fraction

Submitted Feb 19, 2018. Accepted for publication Apr 20, 2018.
doi: 10.21037/qims.2018.04.08
View this article at: http://dx.doi.org/10.21037/qims.2018.04.08

Introduction

Pancreatic ductal adenocarcinoma (PDAC) is one of the leading death causes of cancer worldwide (1). Surgical eradication is the only curative therapy for PDAC. However, most PDAC patients have no chance to receive surgery due to metastasis or local invasion at the diagnosis (2). Therefore, a non-invasive detection and diagnosis method at the early stage of PDAC is needed to improve efficacy and prognosis and to fill in the blank in this area (3,4).

A meta-analysis about imaging tests for staging of PDAC showed that endoscopic ultrasound with fine-needle aspiration (EUS-FNA) was more accurate than CT in T staging and similar in accuracy to CT in assessing resectability (5). However, another meta-analysis showed EUS-FNA had the most frequent rate of adverse reaction such as pancreatitis, a procedural pain, bleeding and perforation compared with other imaging modalities (6). A study has shown that perfusion CT can predict tumor grade of PDAC (7). However, excess exposure to radiation limits its application in evaluating PDAC.

Apparent diffusion coefficient (ADC) derived from diffusion weighted imaging (DWI) can be used to measure the magnitude of hindered water diffusion in tissues. It can be applied to assess tissue microstructure at the early stage of diseases. DWI has been increasingly applied in differentiating benign lesions from malignant ones in the abdomen as MR technology advances. Recently, DWI has been extensively used to detect and characterize pancreatic lesions (2,8-21). However, conflicting results have been reported for ADC values in characterizing pancreatic cancer (PC). Yoshikawa *et al.* (22) reported that PC had a higher ADC value than normal pancreas while some studies showed no significant difference in ADC values between PC and normal pancreatic parenchyma (8,17-19). However, more studies have shown that ADC values of PC are much lower than those of normal pancreas (13-16,20).

The ADC values can reflect Brownian motion of water protons not only in tissue extracellular and intercellular space but also in tissue microcirculation (perfusion effects) (23-25). Perfusion effects may affect the reliability of ADC in characterizing tissue microstructure (26). Based on the intravoxel incoherent motion (IVIM) model, DWI with sufficient b values by using the biexponential analysis enables to separately reflect pure tissue diffusivity and information about microcapillary perfusion (10,23-27). Intravoxel incoherent motion diffusion weighted imaging (IVIM-DWI) can simultaneously provide information about tumor perfusion and diffusion characteristics without using contrast medium, which is meaningful to patients with renal insufficiency (28). Although quantitative parameters derived from IVIM-DWI have been increasingly used to diagnose and differentiate pancreatic lesions recently (10,11,14,18), there has been no report applying them in classifying PDAC into different pathological grades.

Therefore, our study aimed to compare IVIM-DWI derived parameters such as standard ADC ($ADC_{standard}$), pure diffusion coefficient (D_{slow}), pseudodiffusion coefficient (D_{fast}) and perfusion fraction (f) of PDAC with different pathological grades.

Methods

Patients

The study protocol was granted by the Institutional Ethical Review Board of our hospital with a waiver of informed consent. From May 2014 to August 2017, 108 patients with a suspect focal solid pancreatic mass seen in CT examination were referred for inclusion in this study. Eligibility inclusion criteria included: histologically confirmed diagnosis of PDAC by surgery or aspiration biopsy; PDAC with clear pathological grade; without chemotherapy or radiotherapy before MRI examination; and no contraindications to MRI examination. Finally, among 108 patients, 70 were excluded due to various reasons. The case accrual process was summarized in *Figure 1*. Finally, 38 patients (25 men and 13 women, age range: 20–73 years, mean age: 53.2± 14.2 years) with histopathologically confirmed PDAC were enrolled in this study. Of these, 25 patients were proven to be well/moderately differentiated PDAC, and 13 to be poorly differentiated PDAC. All patients in the final cohort underwent routine pancreatic MR imaging and multiple b values DW imaging within 1 week before surgery.

MRI protocols

All MR examinations were performed at a whole-body 3.0T MR scanner (Discovery MR750, GE Medical Systems, Milwaukee, Wis., USA) with a 32-channel body array coil. Routine pancreatic MR imaging protocols included axial respiratory triggering fat-suppressed FSE T_2WI and 3D Liver Acquisition with Volume Acceleration Flex (LAVA Flex) sequence with breath-hold. Pancreatic axial respiratory triggering DW imaging was employed with 15 b values of 0, 10, 20, 40, 60, 80, 100, 150, 200, 400, 800, 1,000, 1,200,

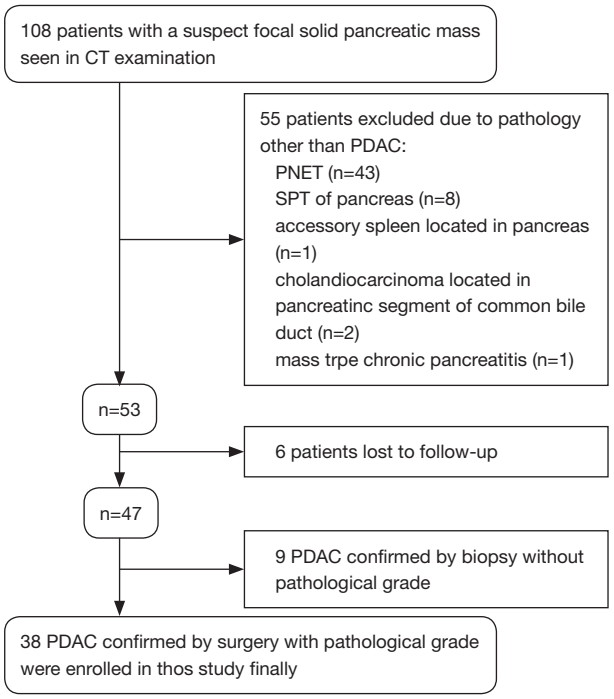

Figure 1 Flowchart shows patient selection process. Of all the 108 patients, 38 were finally enrolled. CT, computed tomography; PDAC, pancreatic ductal adenocarcinoma; PNET, pancreatic neuroendocrine tumor; SPT, solid pseudopapillary tumor; IPMN, intraductal papillary mucinous tumor.

Table 1 Magnetic resonance imaging parameters

Parameters	Sequences		
	Axial FSE T2WI	Axial LAVA flex	DWI
Repetition time, ms	10,000	4.3	6,600
Echo time, ms	70	1.6	81.5–82.3
Slice thickness, mm	4.0	4.0	4.0
Slice gap, mm	0.5	0	1.0
Matrix size, mm^2	320×320	260×210	128×128
Field of view, mm^2	360×360	360×324	380×304
Number of excitation	1.5	1	1-8
Flip angle, °	110	14	90
Bandwidth, Hz/pixel	62.5	200	250
Acquisition Time, s	120–240	11	480–660

Specific number of excitation for each b value is listed as follows: 10 [4], 20 [2], 40 [1], 60 [1], 80 [1], 100 [1], 150 [2], 200 [2], 400 [4], 800 [4], 1,000 [6], 1,200 [6], 1,500 [6], 2,000 [8] s/mm^2. The numbers in brackets represent number of excitation. FSE, fast spin echo; LAVA flex, liver acquisition with volume acceleration flex; DWI, diffusion weighted imaging.

1,500, and 2,000 s/mm^2. The detailed parameters for each sequence were summarized in *Table 1*. No adverse events occurred during MR examinations.

Data analysis

All DWI data were sent to an AW 4.6 workstation provided by the manufacturer (GE Healthcare, Milwaukee, WI) after the examination. All functional parameters maps were post-processed using the MADC programs on AW 4.6 workstation.

Standard ADC value was calculated by mono-exponential model using the total available b values according to the following equation:

$$S(b)/S_0=\exp(-b\cdot ADC) \quad [1]$$

The IVIM parameters were calculated by bi-exponential fitting according to the following equation, suggested by Le Bihan *et al.* (24):

$$S(b)/S_0=f\cdot\exp(-b\cdot D_{fast})+(1-f)\cdot\exp(-b\cdot D_{slow}) \quad [2]$$

Where S(b) corresponds to mean signal intensity on DWI with a certain b value. S_0 is the mean signal intensity on DWI with b value=0. D_{slow} represents pure molecular diffusivity where a physiological perfusion effect is excluded. D_{fast} represents the average blood velocity and mean capillary segment length. f represents the ratio of water movement within capillaries compared with the total volume of water in a voxel. Because D_{fast} is roughly one order of magnitude greater than D_{slow} (29), $-b\cdot D_{fast}$ would be less than −3 at a high b value (>200 s/mm^2), and the term $f\cdot\exp(-b\cdot D_{fast})$ would be less than $0.05f$ and can therefore be neglected. In this case, Eq. [2] can be simplified as follows:

$$S(b)/S_0=(1-f)\cdot\exp(-b\cdot D_{slow}) \quad [3]$$

Hence, for high b values (>200 s/mm^2) S(b) was first fitted to Eq. [3] using a linear model, and then pure diffusion coefficient D_{slow} was calculated. Although we had previously calculated the f value using Eq. [3], its accuracy was not acceptable. Therefore, f was recalculated using Eq. [2]. Then, we fitted S(b) for all b values using Eq. [2] with a fixed D_{slow} value using the nonlinear Levenberg-Marquardt method. When fitting Eq. [2], the initial estimated values for f and D_{fast} were set as the previously calculated f value from Eq. [3] and 10×10^{-3} mm^2/s, respectively. Subsequently, the f and D_{fast} were obtained.

All measurements were performed by experienced radiologists with 11 years of experience in abdominal MRI, who were unaware of the histopathologic results. On DW

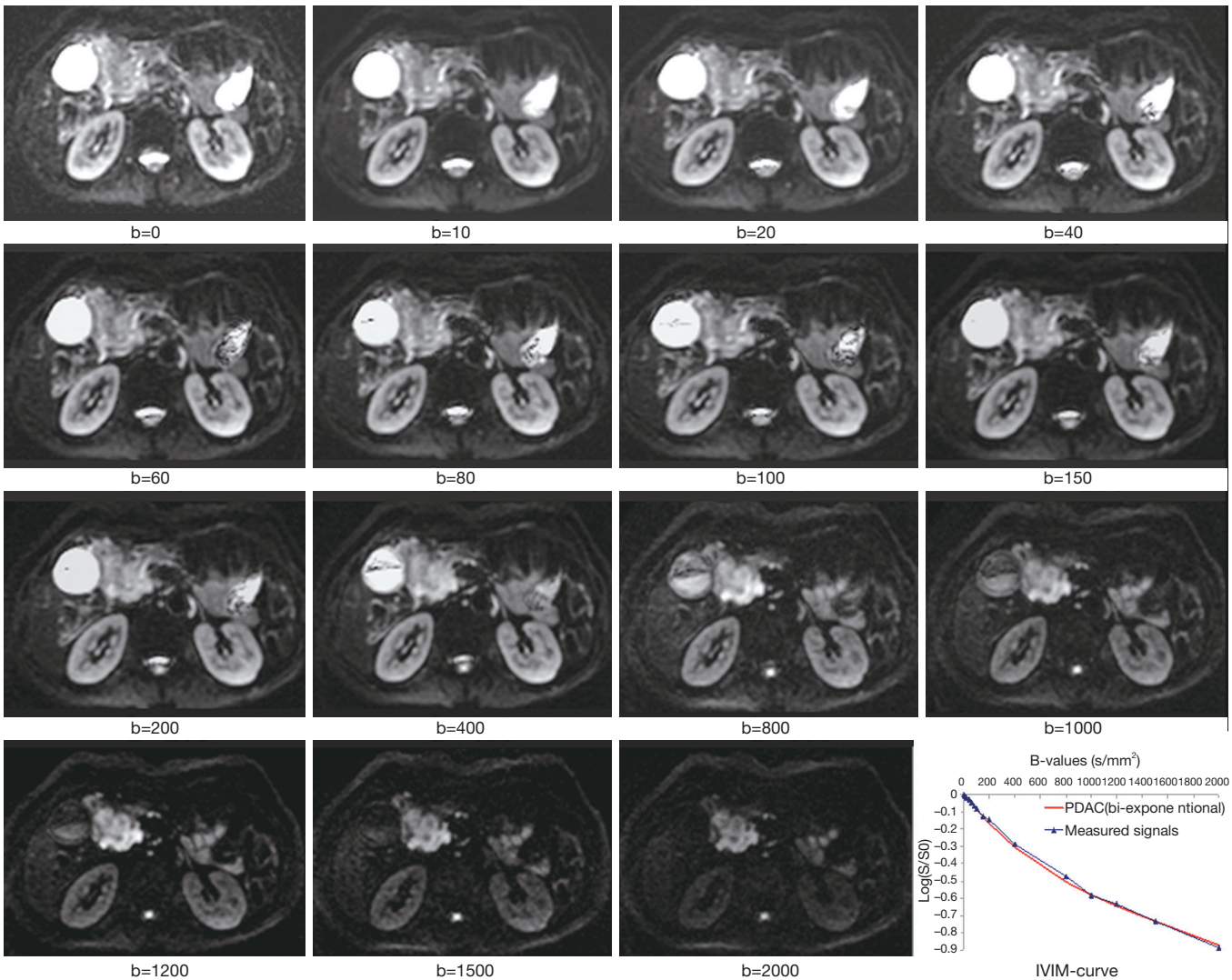

Figure 2 DW images with all b values and IVIM curve map. A poorly differentiated PDAC located in pancreatic head. The tumor shows hyperintensity with different degree on DW images with different b value. The contrast-to-noise ratio increases gradually with the growth of b value. DW, diffusion weighted; IVIM, intravoxel incoherent motion; PDAC, pancreatic ductal adenocarcinoma.

images with b value which showed tumor most clearly among all DW images (*Figure 2*), the largest possible irregular regions of interest (ROIs) for each PDAC were manually drawn along the margin of tumor on three of the largest consecutive lesion slices. More attention was paid to exclude vascular, pancreatic duct, necrosis area within the lesion in process of measurement. Well-matched copies of the ROI were automatically and synchronously generated and appeared on each functional map of $ADC_{standard}$ and IVIM-DWI parameters on corresponding locations by using built-in software (MADC programs on AW 4.6 workstation). The functional parameter maps and ROI setting were shown in *Figure 3A,B,C,D,E*. The average value of the results of three measurements was used as the final result. ROI areas of PDAC ranged from 136 mm^2 (long diameter × short diameter: 20.5 mm × 14.7 mm) to 895 mm^2 (long diameter × short diameter: 46.7 mm × 34.2 mm) with mean areas of 444.75 mm^2 (long diameter × short diameter: 33.9 mm × 25.3 mm).

Statistical analysis

All statistical analyses were performed using SPSS Statistics (version 17.0, SPSS Inc., Chicago, IL) and MedCalc (version 12.3, MedCalc Software, Mariakerke, Belgium). Parameter

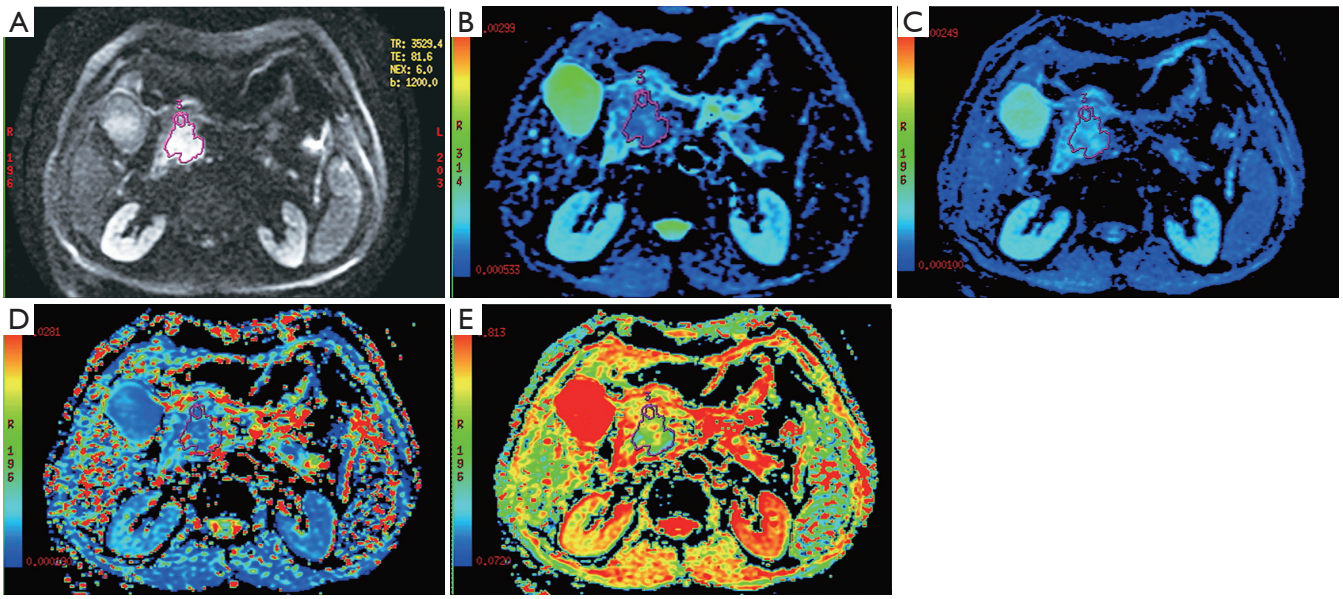

Figure 3 The different functional parameter maps and ROI setting. ROI 3 represents the tumor area. (A) DW image with b value of 1,200 s/mm^2; (B) the functional parameter pseudo color image of $ADC_{standard}$; (C) the functional parameter pseudo color image of D_{slow}; (D) the functional parameter pseudo color image of D_{fast}; (E) the functional parameter pseudo color image of *f*. ROI, regions of interest; DW, diffusion weighted; $ADC_{standard}$, standard apparent diffusion coefficient; D_{slow}, pure diffusion coefficient; D_{fast}, pseudodiffusion coefficient; *f*, perfusion fraction.

values were recorded as means ± standard deviations. Cohen's Kappa statistics (κ) was used to evaluate the inter-rater agreement between the two observers for ADC and IVIM-DWI parameters' measurements. The Independent Sample *t* Test was used for the comparison of $ADC_{standard}$, D_{slow}, D_{fast} and *f* values between well/moderately differentiated PDAC and poorly differentiated PDAC. The diagnostic performances of IVIM-DWI derived parameters were evaluated using receiver operating characteristics (ROC) analysis. The areas under curve (AUC) values were compared, and the cut-off values with the largest Youden index (the sum of sensitivity and specificity) were calculated from the ROC-curves. The P values less than 0.05 were considered statistically significant.

Results

Interobserver agreement in imaging analysis

The measurements of IVIM-DWI parameters and ADC values had the excellent interobserver reproducibility. The interobserver agreement showed the κ value of 0.904 [95% confidence interval (CI), 0.862–0.947] in ADC values. In addition, the agreement between two observers was obtained in D_{slow}, D_{fast}, and *f* values' measurements with κ values of 0.917 (95% CI, 0.885–0.949), 0.818 (95% CI, 0.706–0.930), and 0.889 (95% CI, 0.840–0.939), respectively.

Quantitative analysis of IVIM-DWI parameters

Mean D_{slow} value of well/moderately differentiated PDAC was significantly lower than that of poorly differentiated PDAC (0.540×10^{-3} *vs.* 0.676×10^{-3} mm^2/s, t=5.635, P<0.001). Mean *f* value of well/moderately differentiated PDAC was significantly higher than that of poorly differentiated PDAC (60.3% *vs.* 38.4%, t=5.371, P<0.001). There were no significant differences for $ADC_{standard}$ and D_{fast} between well/moderately differentiated and poorly differentiated PDAC (0.853×10^{-3} *vs.* 0.826×10^{-3} mm^2/s, t=0.670, P=0.507; and 3.448×10^{-3} *vs.* 4.225×10^{-3} mm^2/s, t=0.917, P=0.365; respectively). Detailed results were shown in *Table 2*. The box and whisker plots (*Figure 4*) compared $ADC_{standard}$ and IVIM-DWI parameters between well/moderately differentiated and poorly differentiated PDAC.

ROC analysis of IVIM-DWI parameters

AUC value of *f* was slightly higher than that of D_{slow} (0.894

Table 2 Comparison of IVIM-DWI parameters for well/moderately differentiated and poorly differentiated PDAC

Parameters	Well/moderately differentiated PDAC (n=25)	Poorly differentiated PDAC (n=13)	t	P
$ADC_{standard}$ ($\times10^{-3}$ mm^2/s)	0.853±0.092	0.826±0.151	0.670	0.507
D_{slow} ($\times10^{-3}$ mm^2/s)	0.540±0.038	0.676±0.110	5.635	<0.001
D_{fast} ($\times10^{-3}$ mm^2/s)	3.448±2.367	4.225±2.683	0.917	0.365
f (%)	60.3±8.9	38.4±16.3	5.371	<0.001

IVIM-DWI, intravoxel incoherent motion and diffusion weighted imaging; PDAC, pancreatic ductal adenocarcinoma; $ADC_{standard}$, standard apparent diffusion coefficient; D_{slow}, pure diffusion coefficient; D_{fast}, pseudodiffusion coefficient; f, perfusion fraction.

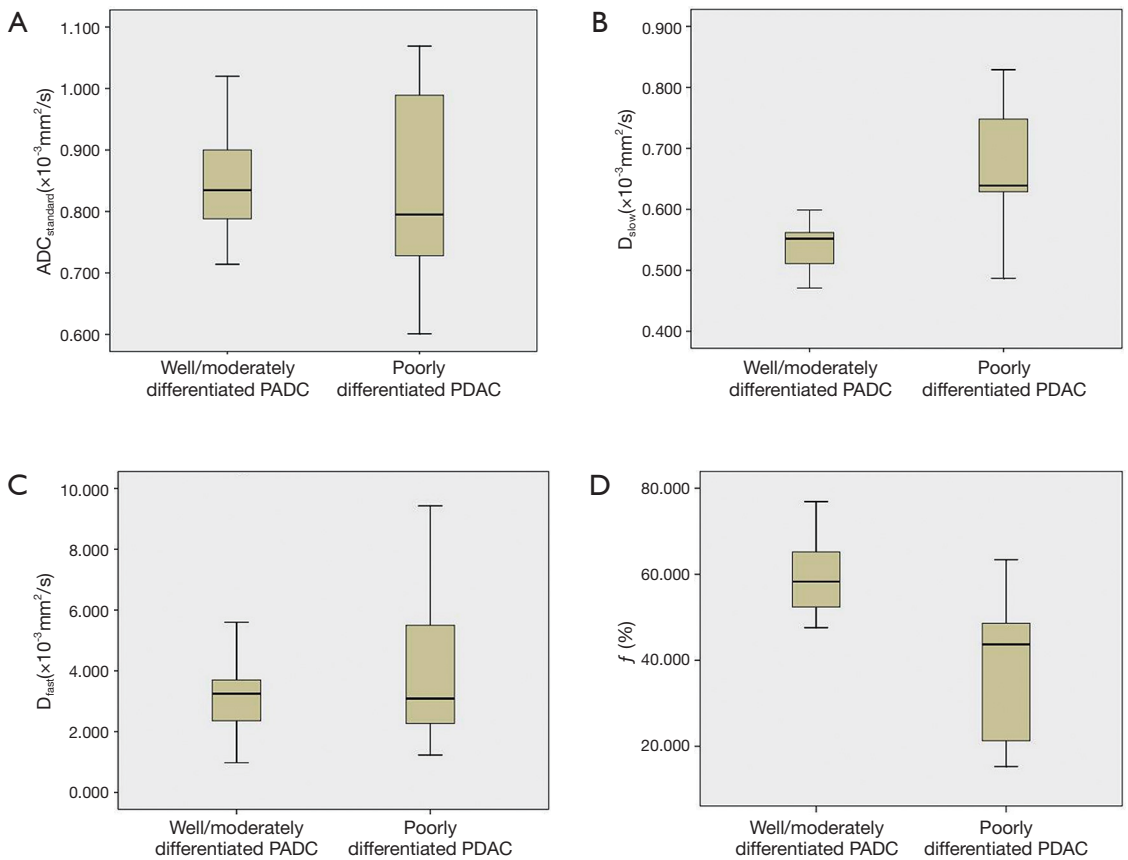

Figure 4 Box and whisker plots comparing IVIM-DWI parameters between well/moderately differentiated and poorly differentiated PDAC. The middle line represents the median. The central box represents the measurements from the lower to the upper quartile (25–75 percentiles). Whiskers indicate the range from the maximum to the minimum parameters measurements. There is no significant difference for $ADC_{standard}$ and D_{fast} between well/moderately differentiated and poorly differentiated PDAC (P=0.507 and 0.365, respectively) (A,C). Mean D_{slow} value of well/moderately differentiated PDAC is significantly lower than that of poorly differentiated PDAC (P<0.001) (B). Mean f value of well/moderately differentiated PDAC is significantly higher than that of poorly differentiated PDAC (P<0.001) (D). IVIM-DWI, intravoxel incoherent motion and diffusion weighted imaging; PDAC, pancreatic ductal adenocarcinoma; $ADC_{standard}$, standard apparent diffusion coefficient; D_{slow}, pure diffusion coefficient; D_{fast}, pseudodiffusion coefficient; f, perfusion fraction.

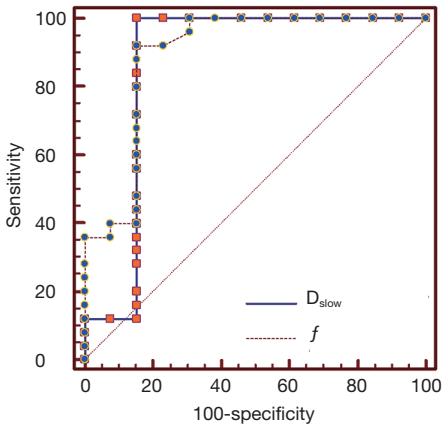

Figure 5 ROC curves of D_{slow} and f for differentiating well/moderately differentiated PDAC from poorly differentiated PDAC. The diagonal line represents the reference line which indicates the results for a test with 50% sensitivity and 50% specificity. The largest AUC can be found for f and closely followed by D_{slow}. ROC, receiver operating characteristic; D_{slow}, pure diffusion coefficient; f, perfusion fraction; PDAC, pancreatic ductal adenocarcinoma.

Table 3 Results of the ROC Analysis for D_{slow} and f

Parameters	AUC (95% CI)	Optimal Cut-off	Sensitivity	Specificity
D_{slow}	0.865 (0.714–0.954)	≤0.599× $\times10^{-3}$ mm^2/s	100%	84.6%
f	0.894 (0.751–0.970)	>49.6%	92.0%	84.6%

ROC, receiver operating characteristic; AUC, area under the ROC curve; D_{slow}, pure diffusion coefficient; f, perfusion fraction.

vs. 0.865). When D_{slow} value was less than or equal to 0.599×10^{-3} mm^2/s, the sensitivity and specificity were 100% and 84.6% respectively for differentiating well/moderately differentiated PDAC from poorly differentiated PDAC. When f value was greater than 49.6%, the sensitivity and specificity were 92.0% and 84.6% respectively for differentiating well/moderately differentiated and poorly differentiated PDAC. ROC curve map was shown in *Figure 5*. The detailed results were listed in *Table 3*.

Discussion

This study showed significant statistical difference in D_{slow} and no significant difference in $ADC_{standard}$ between well/moderately differentiated and poorly differentiated PDAC. The calculation of ADC value usually uses the mono-exponential diffusion model which obeys the Gaussian distribution based on water molecular Brownian motion in vivo. However, water molecular diffusion *in vivo* biologic tissues is much more sophisticated and always deviates from Gaussian law (26). ADC value can be influenced not only by water molecular diffusion in tissue microstructure but also in tissue microcirculation (24,30). Therefore, ADC value is no longer the true diffusion coefficient and cannot reflect sophisticated true diffusion features of water molecular *in vivo* tissues (26). Since the $ADC_{standard}$ value in our study was calculated based on conventional mono-exponential diffusion model, it might not reflect true diffusion features of water molecular *in vivo*.

Quantitative parameters derived from IVIM-DWI can separately reflect tissue diffusivity and tissue microcapillary perfusion (10,23-27). Pure diffusion coefficient (D_{slow}) derived from IVIM-DWI with more and greater b values can better eliminate the perfusion-related diffusion (31). It can better reflect the obstacle of free diffusion of intracellular and extracellular water molecules due to barriers such as membranes, macromolecules, and fibers (23,24,32). Quantitative parameters derived from IVIM-DWI with the higher b values can better reflect the characteristics of the non-Gauss diffusion of water molecules in the tissues (33). An increased number of b values can decrease the CoV (coefficient of variation) of D_{slow} and increase measurement accuracy (34). DWI in our study was performed with 7 high b values (≥200 s/mm^2) and highest b value up to 2,000 s/mm^2. D_{slow} in our study might be closest to the true diffusion characteristics of water molecules in biological tissues. Glandular formation is the crucial morphological characteristic for grading differentiation of PDAC (35). Well/moderately differentiated PDAC shows abundant fibrosis and glandular formation characterized by neoplastic tubular and duct-like structures (35-37). These tubular and duct-like structures contain massive mucus rich in macromolecular protein, which may account for restrained diffusion of water molecules in well/moderately differentiated PDAC. Abundant fibrosis within well/moderately differentiated PDAC can account for more restricted diffusivity of water molecules *in vivo* (8). In contrast, poorly differentiated PDAC characteristically shows limited to no glandular formation and mucus (35). The variability of fibrosis content in poorly differentiated PDAC may have no significant influence on ADC values compared with well/moderately differentiated PDAC (8). This may explain the significant difference in D_{slow} value

between poorly and well/moderately differentiated PDAC observed in our study.

IVIM-DWI with more b values in segment of low b values can get more accurate perfusion-related diffusion (31). DWI in our study was performed with 8 low b values (<200 s/mm^2). The perfusion fraction *f* in our study might better demonstrate perfusion characteristics of PDAC. IVIM-DWI can better demonstrate tumor perfusion characteristics without contrast enhancement (10,23-27). It may be a recommendable substitute for perfusion MR imaging for its risk-free of nephrogenic systemic fibrosis caused by contrast agents and thus is especially suited for patients with contraindications to contrast agents or patients with renal dysfunction (26,28). The perfusion fraction *f* derived from IVIM-DWI describes the volume fraction of intravoxel incoherent signals which comes from the vascular component (23-27,38). The *f* derived from IVIM-DWI showed significant positive correlation with MVD (28). One study demonstrated that well-differentiated PDAC contained higher MVD than poorly differentiated PDAC (39). This could explain that *f* value of well/moderately differentiated PDAC was significantly higher than poorly differentiated PDAC in our study. Due to the high variance and standard deviation (S.D.) in the quantitative analysis (31), no significant difference in D_{fast} was observed between well/moderately differentiated and poorly differentiated PDAC in our study.

The IVIM-DWI derived *f* value showed higher diagnostic performance and closely followed by D_{slow} in differentiating well/moderately differentiated and poorly differentiated PDAC. Wang *et al.* (40) reported that among the three parameters, *f* derived from IVIM-DWI offered the best diagnostic value, followed by D_{slow}, in evaluating liver fibrosis. Both studies showed IVIM technique to be used in the evaluation of abdominal organs. When D_{slow} value was less than or equal to 0.599×10^{-3} mm^2/s and *f* value was greater than 49.6%, both sensitivities were greater than 90% and specificities were 84.6% in differentiating well/moderately differentiated and poorly differentiated PDAC.

Tumor grade of PDAC is a significant prognostic indicator after resection (41,42). High tumor grade has a larger impact on survival than tumor size and lymph node metastases (43). Therefore, a non-invasive imaging method for predicting pathological grade of PDAC before surgery would be helpful to identify the aggressive prognosis of poorly differentiated tumors. This may allow clinicians to optimize therapeutic strategy and further improve prognosis. Our study has shown that D_{slow} and *f* can distinguish well/moderately differentiated and poorly differentiated PDAC. IVIM-DWI can be an important tool for predicting pathological grade of PDAC before surgery.

There were several limitations in our study. First, our study population included only a few poorly differentiated PDAC. However, all patients underwent surgery and acquired histopathological grade in our study. Second, only a respiratory-triggered technique was used, but no pulse or cardiac triggering was performed. This might lead to heterogeneous perfusion parameters maps due to pulsating motion influences caused by large vessels and the high S.D. in the quantitative analysis, which may limit the measurement reproducibility. Third, the influences of fibrosis on IVIM-DWI parameters were not taken into account, which have to be evaluated in further studies. Finally, the b-factor applied in this study may not be optimal. Signal-to-noise ratio (SNR) would decrease with higher b values than 1,000 s/mm^2. Low SNR of image with higher b-value would affect the accuracy of measurement. DWI with more and higher b values would increase sampling time. This needs to be further optimized in order to balance parameter estimation reliability with minimum sampling time.

In conclusion, both IVIM-DWI derived parameters D_{slow} and *f* have high diagnostic performance in distinguishing well/moderately differentiated PDAC from poorly differentiated PDAC. IVIM-DWI may be a promising non-invasive tool for predicting pathological grade of PDAC. Perfusion related parameter *f* derived from IVIM-DWI can be used as an early biomarker in evaluating tumor vascularity of PDAC without use of contrast agents.

Acknowledgements

We thank Xiaocheng Wei (senior engineer, MR Research China, GE healthcare Greater China, Beijing, P. R. China) for designing the MRI scanning protocols and specifying DWI data fitting method used in our study.

Funding: The authors express sincerest gratitude to National Natural Science Foundation of China (Grants NSFC 81220108011, and NSFC 81370039) for grant support.

Footnote

Conflicts of Interest: The authors have no conflicts of interest to declare.

Ethical Statement: Institutional Review Board of our hospital approved this study protocol with a waiver of informed consent.

References

1. Jemal A, Siegel R, Ward E, Hao Y, Xu J, Thun MJ. Cancer statistics, 2009. CA Cancer J Clin 2009;59:225-49.
2. De Robertis R, Tinazzi Martini P, Demozzi E, Dal Corso F, Bassi C, Pederzoli P, D'Onofrio M. Diffusion-weighted imaging of pancreatic cancer. World J Radiol 2015;7:319-28.
3. Gemmel C, Eickhoff A, Helmstadter L, Riemann JF. Pancreatic cancer screening: state of the art. Expert Rev Gastroenterol Hepatol 2009;3:89-96.
4. Klapman J, Malafa MP. Early detection of pancreatic cancer: why, who, and how to screen. Cancer Control 2008;15:280-7.
5. Treadwell JR, Zafar HM, Mitchell MD, Tipton K, Teitelbaum U, Jue J. Imaging Tests for the Diagnosis and Staging of Pancreatic Adenocarcinoma: A Meta-Analysis. Pancreas 2016;45:789-95.
6. Toft J, Hadden WJ, Laurence JM, Lam V, Yuen L, Janssen A, Pleass H. Imaging modalities in the diagnosis of pancreatic adenocarcinoma: A systematic review and meta-analysis of sensitivity, specificity and diagnostic accuracy. Eur J Radiol 2017;92:17-23.
7. D'Onofrio M, Gallotti A, Mantovani W, Crosara S, Manfrin E, Falconi M, Ventriglia A, Zamboni GA, Manfredi R, Pozzi Mucelli R. Perfusion CT can predict tumoral grading of pancreatic adenocarcinoma. Eur J Radiol 2013;82:227-33.
8. Wang Y, Chen ZE, Nikolaidis P, McCarthy RJ, Merrick L, Sternick LA, Horowitz JM, Yaghmai V, Miller FH. Diffusion-weighted magnetic resonance imaging of pancreatic adenocarcinomas: association with histopathology and tumor grade. J Magn Reson Imaging 2011;33:136-42.
9. Jang KM, Kim SH, Kim YK, Park MJ, Lee MH, Hwang J, Rhim H. Imaging features of small (≤3cm) pancreatic solid tumors on gadoxetic-acid-enhanced MR imaging and diffusion-weighted imaging: an initial experience. Magn Reson Imaging 2012;30:916-25.
10. Klauss M, Lemke A, Grünberg K, Simon D, Re TJ, Wente MN, Laun FB, Kauczor HU, Delorme S, Grenacher L, Stieltjes B. Intravoxel incoherent motion MRI for the differentiation between mass forming chronic pancreatitis and pancreatic carcinoma. Invest Radiol 2011;46:57-63.
11. Klauss M, Gaida M, Lemke A, Grünberg K, Simon D, Wente MN, Delorme S, Kauczor HU, Grenacher L, Stieltjes B. Fibrosis and pancreatic lesions: counterintuitive behavior of the diffusion imaging-derived structural diffusion coefficient D. Invest Radiol 2013;48:129-33.
12. Wiggermann P, Grützmann R, Weissenböck A, Kamusella P, Dittert DD, Stroszczynski C. Apparent diffusion coefficient measurements of the pancreas, pancreas carcinoma, and mass-forming focal pancreatitis. Acta Radiol 2012;53:135-9.
13. Hao JG, Wang JP, Gu YL, Lu ML. Importance of b value in diffusion weighted imaging for the diagnosis of pancreatic cancer. World J Gastroenterol 2013; 19:6651-5.
14. Kim H, Arnoletti PJ, Christein J, Heslin MJ, Posey JA 3rd, Pednekar A, Mark Beasley T, Morgan DE. Pancreatic adenocarcinoma: a pilot study of quantitative perfusion and diffusion-weighted breath-hold magnetic resonance imaging. Abdom Imaging 2014;39:744-52.
15. Yao XZ, Yun H, Zeng MS, Wang H, Sun F, Rao SX, Ji Y. Evaluation of ADC measurements among solid pancreatic masses by respiratory-triggered diffusion-weighted MR imaging with inversion-recovery fat-suppression technique at 3.0T. Magn Reson Imaging 2013;31:524-8.
16. Fukukura Y, Takumi K, Kamimura K, Shindo T, Kumagae Y, Tateyama A, Nakajo M. Pancreatic Adenocarcinoma: Variability of Diffusion-weighted MR Imaging Findings. Radiology 2012;263:732-40.
17. Barral M, Sebbag-Sfez D, Hoeffel C, Chaput U, Dohan A, Eveno C, Boudiaf M, Soyer P. Characterization of focal pancreatic lesions using normalized apparent diffusion coefficient at 1.5-Tesla: preliminary experience. Diagn Interv Imaging 2013;94:619-27.
18. Kang KM, Lee JM, Yoon JH, Kiefer B, Han JK, Choi BI. Intravoxel incoherent motion diffusion-weighted MR imaging for characterization of focal pancreatic lesions. Radiology 2014;270:444-53.
19. Lee SS, Byun JH, Park BJ, Park SH, Kim N, Park B, Kim JK, Lee MG. Quantitative analysis of diffusion-weighted magnetic resonance imaging of the pancreas: usefulness in characterizing solid pancreatic masses. J Magn Reson Imaging 2008;28:928-36.
20. Muraoka N, Uematsu H, Kimura H, Imamura Y, Fujiwara Y, Murakami M, Yamaguchi A, Itoh H. Apparent diffusion coefficient in pancreatic cancer: characterization and histopathological correlations. J Magn Reson Imaging 2008;27:1302-8.
21. Ichikawa T, Erturk SM, Motosugi U, Sou H, Iino H, Araki T, Fujii H. High-b value diffusion-weighted MRI for detecting pancreatic adenocarcinoma: preliminary results. AJR Am J Roentgenol 2007;188:409-14.
22. Yoshikawa T, Kawamitsu H, Mitchell DG, Ohno Y, Ku Y, Seo Y, Fujii M, Sugimura K. ADC measurement of abdominal organs and lesions using parallel imaging technique. AJR Am J Roentgenol 2006;187:1521-30.

23. Le Bihan D, Breton E, Lallemand D, Grenier P, Cabanis E, Laval-Jeantet M. MR imaging of intravoxel incoherent motions: application to diffusion and perfusion in neurologic disorders. Radiology 1986;161: 401-7.
24. Le Bihan D, Breton E, Lallemand D, Aubin ML, Vignaud J, Laval-Jeantet M. Separation of diffusion and perfusion in intravoxel incoherent motion MR imaging. Radiology 1988;168:497-505.
25. Le Bihan D, Turner R, Moonen CT, Pekar J. Imaging of diffusion and microcirculation with gradient sensitization: design, strategy, and significance. J Magn Reson Imaging 1991;1:7-28.
26. Iima M, Le Bihan D. Clinical Intravoxel Incoherent Motion and Diffusion MR Imaging: Past, Present, and Future. Radiology 2016;278:13-32.
27. Koh DM, Collins DJ, Orton MR. Intravoxel incoherent motion in body diffusion-weighted MRI: reality and challenges. AJR Am J Roentgenol 2011;196:1351-61.
28. Lee HJ, Rha SY, Chung YE, Shim HS, Kim YJ, Hur J, Hong YJ, Choi BW. Tumor perfusion-related parameter of diffusion-weighted magnetic resonance imaging: correlation with histological microvessel density. Magn Reson Med 2014;71:1554-8.
29. Le Bihan D. Intravoxel incoherent motion perfusion MR imaging: a wake-up call. Radiology 2008;249:748-52.
30. Chandarana H, Lee VS, Hecht E, Taouli B, Sigmund EE. Comparison of biexponential and monoexponential model of diffusion weighted imaging in evaluation of renal lesions: preliminary experience. Invest Radiol 2011;46:285-91.
31. Lemke A, Stieltjes B, Schad LR, Laun FB. Toward an optimal distribution of b values for intravoxel incoherent motion imaging. Magn Reson Imaging 2011;29:766-76.
32. Muhi A, Ichikawa T, Motosugi U, Sano K, Matsuda M, Kitamura T, Nakazawa T, Araki T. High-b-value diffusion-weighted MR imaging of hepatocellular lesions: estimation of grade of malignancy of hepatocellular carcinoma. J Magn Reson Imaging 2009;30:1005-11.
33. Anderson SW, Barry B, Soto JA, Ozonoff A, O'Brien M, Jara H. Quantifying hepatic fibrosis using a biexponential model of diffusion weighted imaging in ex vivo liver specimens. Magn Reson Imaging 2012;30:1475-82.
34. Li YT, Cercueil JP, Yuan J, Chen W, Loffroy R, Wang YX. Liver intravoxel incoherent motion (IVIM) magnetic resonance imaging: a comprehensive review of published data on normal values and applications for fibrosis and tumor evaluation. Quant Imaging Med Surg 2017;7:59-78.
35. Klöppel G, Lingenthal G, von Bülow M, Kern HF. Histological and fine structural features of pancreatic ductal adenocarcinomas in relation to growth and prognosis: studies in xenografted tumours and clinico-histopathological correlation in a series of 75 cases. Histopathology 1985;9:841-56.
36. Jaster R, Emmrich J. Crucial role of fibrogenesis in pancreatic diseases. Best Pract Res Clin Gastroenterol 2008;22:17-29.
37. Erkan M, Hausmann S, Michalski CW, Schlitter AM, Fingerle AA, Dobritz M, Friess H, Kleeff J. How fibrosis influences imaging and surgical decisions in pancreatic cancer. Front Physiol 2012;3:389.
38. Hwang EJ, Lee JM, Yoon JH, Kim JH, Han JK, Choi BI, Lee KB, Jang JY, Kim SW, Nickel MD, Kiefer B. Intravoxel incoherent motion diffusion-weighted imaging of pancreatic neuroendocrine tumors: prediction of the histologic grade using pure diffusion coefficient and tumor size. Invest Radiol 2014;49:396-402.
39. Barău A, Ruiz-Sauri A, Valencia G, Gómez-Mateo Mdel C, Sabater L, Ferrandez A, Llombart-Bosch A. High microvessel density in pancreatic ductal adenocarcinoma is associated with high grade. Virchows Arch 2013;462:541-6.
40. Wáng YXJ, Deng M, Li YT, Huang H, Leung JCS, Chen W, Lu PX. A Combined Use of Intravoxel Incoherent Motion MRI Parameters Can Differentiate Early-Stage Hepatitis-b Fibrotic Livers from Healthy Livers. SLAS Technol 2017. [Epub ahead of print]. doi: 10.1177/2472630317717049.
41. Lim JE, Chien MW, Earle CC. Prognostic factors following curative resection for pancreatic adenocarcinoma: a population based, linked database analysis of 396 patients. Ann Surg 2003;237:74-85.
42. Kuhlmann KF, de Castro SM, Wesseling JG, ten Kate FJ, Offerhaus GJ, Busch OR, van Gulik TM, Obertop H, Gouma DJ. Surgical treatment of pancreatic adenocarcinoma; actual survival and prognostic factors in 343 patients. Eur J Cancer 2004;40:549-58.
43. Wasif N, Ko CY, Farrell J, Wainberg Z, Hines OJ, Reber H, Tomlinson JS. Impact of tumor grade on prognosis in pancreatic cancer: should we include grade in AJCC staging? Ann Surg Oncol 2010;17:2312-20.

Cite this article as: Ma W, Zhang G, Ren J, Pan Q, Wen D, Zhong J, Zhang Z, Huan Y. Quantitative parameters of intravoxel incoherent motion diffusion weighted imaging (IVIM-DWI): potential application in predicting pathological grades of pancreatic ductal adenocarcinoma. Quant Imaging Med Surg 2018;8(3):301-310. doi: 10.21037/qims.2018.04.08

